where the ligand is mostly protonated at pH 7.4 is that any uncertainties in the estimation have little effect on the pM calculation, since the ligand deprotonation reaction is insignificant.

Formation constants and pM values of coprogen and ferricrocin are given in Table I. The numbers are in accord with our expectations based on simple hydroxamates and comparisons with values of related tris(hydroxamate) siderophores.[35] From β_{110} and K^*, it is apparent that coprogen has a somewhat higher affinity for iron than any of the ferrichrome-type ligands. This observation may be explained (as can the greater acidity of the free ligand) by conjugation of the C=C bond with the hydroxamate group; this increases the electron density at the carbonyl oxygen through both inductive and resonance effects.

Formation constant data have been used for identifying which ligands could be useful in the treatment of iron-overload diseases. The most important criterion determining whether further tests should be done is that the ligand be capable of removing iron from the iron-transport protein, transferrin. Since coprogen and ferricrocin both have a significantly higher affinity for iron than transferrin (which has a pM of 23.6), both ligands are thermodynamically able to abstract iron from the protein. Whether they are kinetically able to do so is being examined currently.

Electrochemistry. Redox potentials for coprogen and ferricrocin were found to be −691 and −656 (±7) mV vs. SCE, respectively, or −447 and −412 mV vs. the normal hydrogen electrode (NHE). No significant shift was observed with different scan rates from 50 to 200 mV/s or with different concentrations of electroactive species. Peak-to-peak separations of 60–69 mV indicate that the electrochemical reactions are reversible or nearly reversible under our conditions. Comparison of these redox potentials to those of other hydroxamate siderophores shown in Table I indicate that all fall in the same range, approximately −0.40 to −0.45 V vs. NHE. These numbers have implications for the mechanism of release of iron(III) from coprogen and ferricrocin, since in the related ferrichrome system[5] it is believed that ferric ferrichrome is reduced to ferrous ferrichrome, followed by release of iron(II). A similar mechanism may be operating with coprogen and ferricrocin; an oxidoreductase capable of reducing both of these compounds has been reported for *N. crassa*.[6]

Summary

The electrochemical and thermodynamic properties of coprogen and ferricrocin have been found to be similar to those of other hydroxamate siderophores. Ferricrocin, as with other ferrichrome-type siderophore complexes, exists as the Λ isomer and possesses comparable formation constants and redox potentials. In contrast, coprogen adopts a Δ configuration in solution and has a somewhat higher affinity for iron(III) than other hydroxamates.

Acknowledgment. This work was supported by the NIH (Grant AI 11744 and, in part, HL 24775). We thank the Bio-organic, Biomedical Mass Spectrometry Resource (A. L. Burlingame, Director) supported by NIH (RR00719) from Division of Research Resources. An American Cancer Society postdoctoral fellowship (1979–1980) is gratefully acknowledged by G.B.W. We are indebted to Professor Zähner for his gifts of compounds.

Registry No. Desferricoprogen, 30315-65-2; coprogen, 31418-71-0; ferricrocin, 23086-46-6; ferrichrome, 15630-64-5; ferrichrysin, 18972-10-6; ferrioxamine B, 14836-73-8; EDTA, 60-00-4.

UV Photoelectron Spectra and Electronic Structure of $(\eta^5\text{-}C_5H_5)(CO)_2FeB_2H_5$. Comparison of the Fe–B Bonding with the Fe–C Bonding in $(CO)_4FeC_2H_4$

Roger L. DeKock,[†] Prabodh Deshmukh,[†] Thomas P. Fehlner,*[†] Catherine E. Housecroft,[†] Jeffrey S. Plotkin,[‡] and Sheldon G. Shore*[‡]

Contribution from the Departments of Chemistry, University of Notre Dame, Notre Dame, Indiana 46556, and The Ohio State University, Columbus, Ohio 43210. *Received April 29, 1982*

Abstract: The valence level photoelectron spectrum of $(\eta^5\text{-}C_5H_5)(CO)_2FeB_2H_5$, I, has been measured in the gas phase with He I and Ne I radiation. The observed bands are assigned on the basis of model compound spectra, intensity changes with photon energy, and relative band areas. Molecular orbital calculations of the Fenske–Hall type on I as well as on $(CO)_4FeC_2H_4$, II, and the free ligands $B_2H_5^-$ and C_2H_4 corroborate the assignment of the spectrum as well as permit the detailed comparison of the Fe–B and Fe–C interactions in I and II. This comparison demonstrates that the B_2H_5 fragment in I can be considered as a $B_2H_4^{2-}$ side-on bound π ligand with a proton in the π lobe opposite the metal. The role of this proton is an active one in that contour plots show that the electron density distribution of the primary Fe–B interaction orbital of I is very different from that of the Fe–C interaction orbitals in II; namely, the Fe–B interaction is more aptly described as a closed three-center two-electron bond. Finally, extended Hückel calculations are used to demonstrate that the qualitative similarities and differences observed for $B_2H_5^-$ and C_2H_4 are apparent in the known higher homologues as well.

Despite the fact that boranes are considered to be "electron-deficient" compounds and exhibit the requisite electron acceptor properties, there are well-documented instances in which boranes act as electron donors.[1] Thus, for example, the electron-rich B–B bond in the pentagonal base of B_6H_{10} acts as an electron donor toward the $Fe(CO)_4$ fragment in the same manner as the C–C π bond in C_2H_4.[2] In recent years, more and more examples of borane fragments, isoelectronic with hydrocarbon π ligands, have

[†] University of Notre Dame.
[‡] The Ohio State University.

(1) Shore, S. G. In "Boron Hydride Chemistry"; Muetterties, E. L., Ed.; Academic Press: New York, 1975; p 79.
(2) Davison, A.; Traficante, D. D.; Wreford, S. S. *J. Am. Chem. Soc.* 1974, *96*, 2802.

0002-7863/83/1505-0815$01.50/0

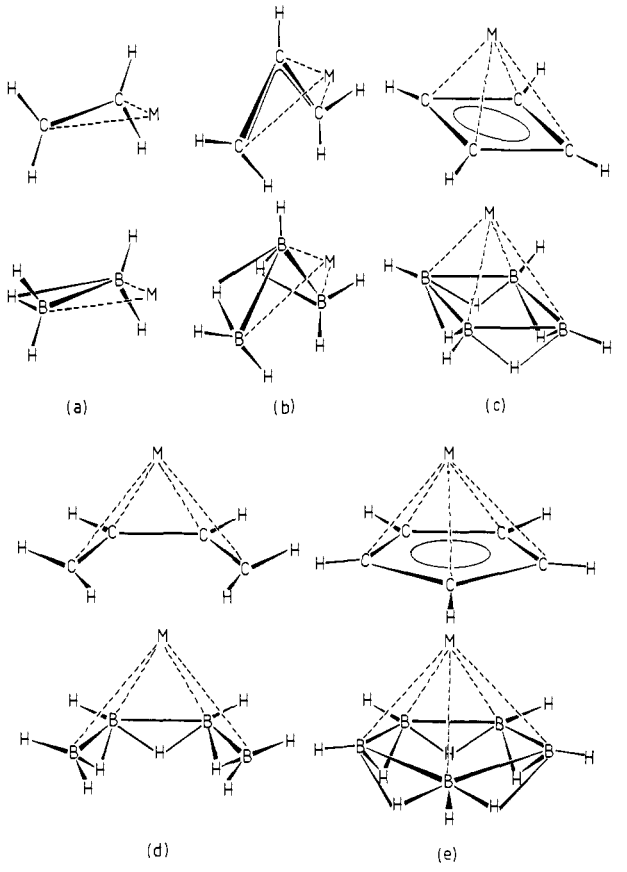

Figure 1. Schematic drawings of the metal–ligand geometry in hydrocarbon π complexes and known borane analogues: (a) CpFe $(CO)_2B_2H_5$,[3] (b) $L_2PtB_3H_7$,[4] (c) $(CO)_3FeB_4H_8$,[5] (d) $L_2(CO)IrB_4H_9$,[6] (e) $CpFeB_5H_{10}$.[7]

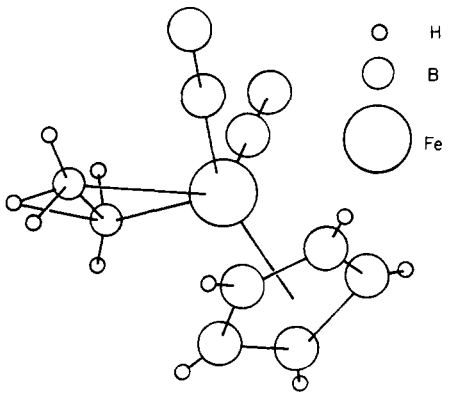

Figure 2. Schematic drawing of the geometrical structure of CpFe-$(CO)_2B_2H_5$, I.

been described in the literature (Figure 1).[3-7] In each case, the borane ligand with n borons can be generated from the hydrocarbon by formally removing a proton from each carbon nucleus and by putting either n or $(n-1)$ protons in appropriate bridging locations.

The direct comparison of electronic spectral properties of compounds differing only in the spatial location of one or more protons produces significant information on the nature of the bonding in both compounds, e.g., C_2H_4 vs. B_2H_6.[8,9] In this work we present a detailed comparison of the UV photoelectron spectra (UV-PES) and quantum chemical calculations utilizing the Fenske–Hall approach for representative compounds containing

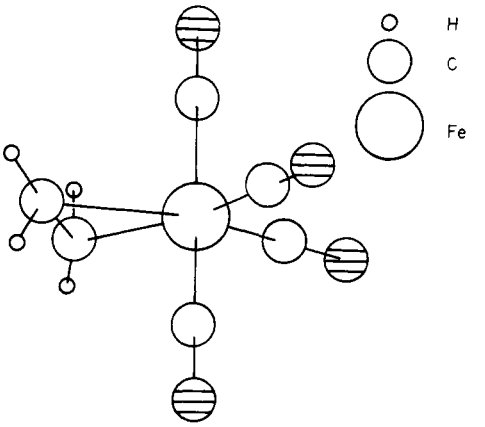

Figure 3. Schematic drawing of the geometrical structure of $(CO)_4Fe-C_2H_4$, II.

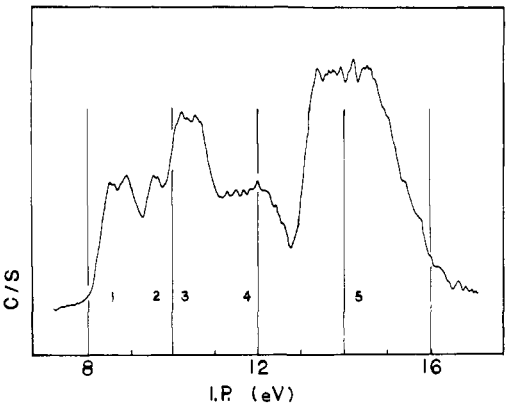

Figure 4. He(I) gas-phase photoelectron spectrum of I.

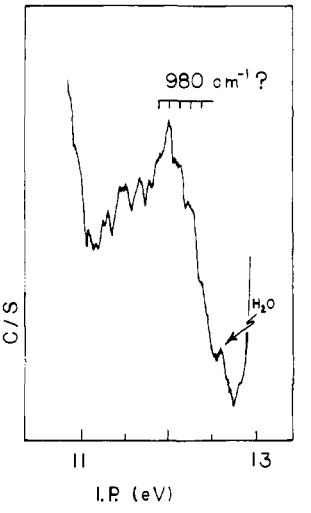

Figure 5. Band 4 of the spectrum of I shown with expanded scale.

(3) Medford, G.; Shore, S. G. *J. Am. Chem. Soc.* **1978**, *100*, 3953. Plotkin, J. S.; Shore, S. G. *J. Organomet. Chem.* **1979**, *182*, C15. Shore, S. G.; Plotkin, J. S.; Huffman, J. C.; Long, G. J.; Fehlner, T. P.; DeKock, R. L. "Abstracts of Papers", 181st National Meeting of the American Chemical Society, Atlanta, GA 1981; American Chemical Society: Washington, DC, 1981; INORG 104.

(4) Kane, A. R.; Muetterties, E. L. *J. Am. Chem. Soc.* **1971**, *93*, 1041. Gugenberger, L. J.; Kane, A. R.; Muetterties, E. L. *Ibid.* **1972**, *94*, 5665.

(5) Greenwood, N. N.; Savory, C. G.; Grimes, R. N.; Sneddon, L. G.; Davison, A.; Wreford, S. S. *J. Chem. Soc., Chem. Commun.* **1974**, 718.

(6) Boocock, S. K.; Toft, M. J.; Shore, S. G.; Huffman, J. C.; Folting, K. "Abstracts of Papers", 182nd National Meeting of the American Chemical Society, New York, Aug 1981, American Chemical Society; Washington, DC, 1981; INORG 149.

(7) Weiss, R.; Grimes, R. N. *Inorg. Chem.* **1979**, *18*, 3291.

(8) Brundle, C. R.; Robin, M. B.; Basch, H.; Pinsky, M.; Bond, A. *J. Am. Chem. Soc.* **1970**, *92*, 3863.

(9) DeKock, R. L.; Wong, K. S.; Fehlner, T. P. *Inorg. Chem.* **1982**, *21*, 3203.

Table I. Vertical Ionization Potentials, Relative Band Areas, Band Characters, and Fenske–Hall Computational Results for $(\eta^5\text{-}C_5H_5)(CO)_2FeB_2H_5$

band[a]	IP,[b] eV	A/E[c]	A_{Ne}/A_{He}[e]	IP's[f] per band	band character (exptl)	IP,[g] eV (calcd)	orbital character (calcd)
						2.15 LUMO	
1	8.61	0.25	0.88	1	Fe (3d)	11.41 HOMO	Fe (3d)
	8.93	0.30	0.81	1	Fe (3d)	11.89	Fe (3d)
2	9.63	0.31	1.13	1	Fe (3d), B (2p)	12.16 (MO 30)[h]	Fe (3d), B (2p)
3	10.40	1.00[d]	1.00[d]	2	πCp	14.99	πCp (C2p)
						15.13	πCp (C2p)
4	11.45	1.18	1.85	2	Fe (3d), B (2p)	13.60 (MO 29)[h]	Fe (3d), B (2p)
	11.99				B (2p), H (1s)	17.43	B (2p), H (1s)
5	13.94	4.71	0.63	>8	CO (5σ, 1π)	18.2–18.5 (3)	B (2p), H (1s)
					Cp		
					BH		
						18.8–19.2 (2)	Cp
						19.4–22.7 (9)	CO (5σ, 1π)
							Cp
							B (2s)
						24.2–43.8 (11)	B, C, O (2s)

[a] See Figure 1. [b] Vertical IP's. [c] Band area over electron energy (HeI). [d] Defined as 1.0. [e] NeI refers to 736 Å and HeI refers to 584-Å radiation. [f] According to assignment described in text. [g] Negative of Fenske–Hall eigenvalues; number of eigenvalues, if more than one, are in parentheses. [h] Eigenvalue number of 32 MO's beginning with lowest energy value.

the $B_2H_5^-$ and C_2H_4 fragments as ligands. In addition we give a qualitative molecular orbital (MO) description in the manner of Hoffmann[10] of the ligand properties of the rest of the borane fragments shown in Figure 1 relative to those of the analogous hydrocarbons. These comparative studies reveal distinct similarities between the bonding of analogous borane and hydrocarbon ligands to a transition metal. However, they also demonstrate some significant differences that can be attributed to the presence of the bridging hydrogens in the borane.

Results and Discussion

The two molecules containing the $B_2H_5^-$ and C_2H_4 ligands, $(\eta^5\text{-}C_5H_5)(CO)_2FeB_2H_5$, I, and $(CO)_4FeC_2H_4$, II, are shown in detail in Figures 2 and 3, respectively. The geometrical structure of the former has been presented previously,[3] and the structure of the latter is well-known and has been the subject of considerable discussion.[11,12] In addition the photoelectron spectrum of II has been reported.[13] Consequently, the majority of this section is devoted to an analysis of the electronic structure of FpB_2H_5 $[(\eta^5\text{-}C_5H_5)(CO)_2Fe = Fp]$.

Photoelectron Spectrum. The UV–PE spectrum of I is displayed in Figures 4 and 5 and the data are gathered in Table I. Although the spectrum is complex, comparison with spectra of model compounds yields a straightforward qualitative assignment. The spectrum of $Fe(CO)_5$ demonstrates that bands 1 and 5 of I contain Fe 3d and CO ionizations, respectively. The spectrum of $FpCH_3$[14] shows that band 3 is due to ionizations associated with the C_5H_5 ligand. In addition, the relative areas of bands 1, 2, and 3 in I compared to the analogous bands in $FpCH_3$ suggest that bands 1 and 2 contain no more than 3 IP's. The envelope of band 1 shows that it contains 2 IP's. Note that $FpCH_3$ exhibits no ionizations in the region from 11 to 13 eV.[14] Comparison of relative band areas in the He I and Ne I spectra suggests bands 1 and 2 have mainly Fe 3d character, band 4 has B or BH character, and band 5 has CO character. Band 4, which is shown in more detail in Figure 5, clearly contains at least two ionization events and the relative area suggests two only. There is evidence of fine structure on both bands; however, only a tentative assignment of a progression of 980 cm^{-1} on the higher IP band is possible with the present data. On this basis we propose that the high IP component of band 4 (11.99 eV) is due to ionization of an orbital associated primarily with the terminal BH bonding of the B_2H_5 fragment. Thus, it is similar to the lowest IP of the model compound B_2H_6 (11.81 eV, 850 cm^{-1}).[8] By difference, we assign the low IP component of band 4 (11.45 eV) to ionization of an orbital associated with the metal–boron interaction. Unfortunately, because of strongly overlapping bands, the He I/Ne I data cannot be used to support this assignment of band 4. A summary of the empirical assignment is given in Table I.

Table II. Fenske–Hall Computational Results and Existing UV-PES Data for $C_2H_4Fe(CO)_4$

IP,[a] eV calcd	orbital character	IP, (eV)[d] (lit.)	IP's per band	band character
−0.55 LUMO				
9.03 HOMO	Fe (3d)	8.38	2	Fe (3d)
9.12 (MO 29)[b]	Fe (3d), π^* (CC)			
9.62	Fe (3d)	9.23	2	Fe (3d)
9.93	Fe (3d)			
12.94 (MO 26)	Fe (3d), π(CC)	10.56	1	π (CC)
18.18 (MO 22)	CH	12.48	1	CH
16.4–21.7 (14)[c]	CO (5σ, 1π) C (2p) H (1s)	14–16		CO, C_2H_4
22.9–42.8 (10)	C, O (2s)			

[a] Negative of calculated F-H eigenvalues. [b] Eigenvalue number of 30 MO's beginning with lowest energy value. [c] Number of eigenvalues if more than one are in parentheses. [d] Reference 13.

Quantum Chemical Calculations. Molecular orbital calculations of the Fenske–Hall type[15] were carried out on I, II, and B_2H_6 as well as the fragments B_2H_5 and C_2H_4 in both the geometry of the free ligands and that of the ligands in the two metal complexes. The energy level diagram for the complexes and ligands is given in Figure 6 and the information for the metal complexes is summarized and compared to the UV–PE spectra in Tables I and II. The comparison of the MO eigenvalues with the UV–PES IP's is carried out within the framework of Koopmans' theorem.[16] To evaluate the extent of agreement between spectra and calculations, the orbital character described in terms of the coefficients of the atomic orbitals in the LCAO–MO's is compared to the empirical

(10) Hoffmann, R. *Science (Washington, D.C.)* **1981**, *211*, 995.
(11) Dewar, M. J. S. *Bull. Soc. Chim. Fr.* **1951**, *18*, C71. Chatt, J.; Duncanson, L. A. *J. Chem. Soc.* **1953**, 2939.
(12) See: Mingos, D. M. P. *Adv. Organomet. Chem.* **1977**, *15*, 1 and references therein.
(13) Van Dam, H.; Oskam, A. *J. Electron Spectrosc. Relat. Phenom.* **1979**, *17*, 357.
(14) Symon, D. A.; Waddington, T. C. *J. Chem. Soc., Dalton Trans.* **1975**, 2140. Green, J. C.; Jackson, S. E. *Ibid.* **1976**, 1698. Lichtenberger, D. L.; Fenske, R. F. *J. Am. Chem. Soc.* **1976**, *98*, 50. Fabian, B. D.; Fehlner, T. P.; Hwang, L.-S., J.; Labinger, J. A. *J. Organomet. Chem.* **1980**, *191*, 409.
(15) Hall, M. B.; Fenske, R. F. *Inorg. Chem.* **1972**, *11*, 768. Hall, M. B. Ph.D. Thesis, University of Wisconsin, Madison, WI, 1971. Fenske, R. F. *Pure Appl. Chem.* **1971**, *27*, 61.
(16) For a leading reference, see: Calabro, D. C.; Lichtenberger, D. L. *Inorg. Chem.* **1980**, *19*, 1732.

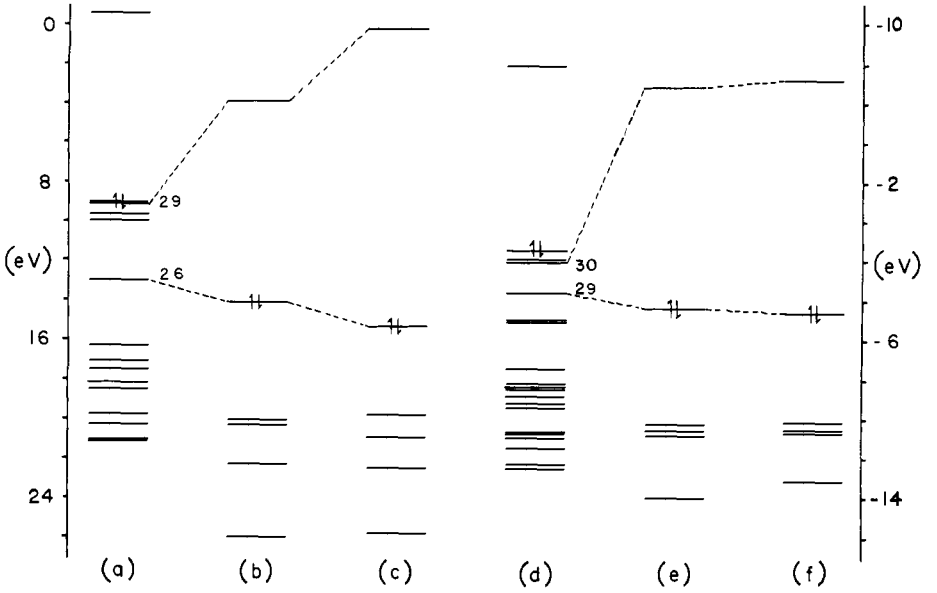

Figure 6. Comparison of eigenvalue spectra for (a) II, (b) C_2H_4 having the same structure as the C_2H_4 fragment in II, (c) C_2H_4 in the planar form of the free ligand, (d) I, (e) $B_2H_5^-$ having the same structure as the B_2H_5 fragment in I, (f) $B_2H_5^-$ having the same structure as the B_2H_5 fragment in B_2H_6. The energy scale for (a)–(d) is at the left while that for (e) and (f) is at the right of the figure.

band characters presented above. Quantitative agreement is neither expected nor found (Table I). However, with one excpetion, the ordering of filled orbitals agrees with the assigned spectrum. The exception is that MO 29 (−13.60 eV) is less stable than the Cp MO's (−14.99, −15.13 eV) whereas the equivalent IP of MO 29 is assigned to band 4 (11.45 eV) which has a higher IP than the Cp IP's (10.40 eV). This instance of the "failure" of Koopmans' theorem in no way affects the validity of comparing the spectra of FpB_2H_5 and $(CO)_4FeC_2H_4$ on the one hand and the calculations on FpB_2H_5 and $(CO)_4FeC_2H_4$ on the other.

In Table II the results of our calculations on $(CO)_4FeC_2H_4$ are compared with previously reported UV–PES results on this molecule.[13] Here the ordering of spectral bands and calculated eigenvalues agree well. It is important to note that the Koopmans' IP of the Fe–C_2H_4 interaction orbital (MO 26, 12.94 eV) is considerably *higher* than the experimental IP (10.56 eV) and that the splitting between MO 26 and the lowest CH type orbital (MO 22) is much larger (5.24 eV) than the experimental splitting (1.92 eV). This suggests that the empirical assignment of I is correct as given above; i.e., the calculated splitting between MO 29 and the lowest BH type orbital is 3.83 eV whereas the experimental splitting is 0.54 eV. Thus, the discrepancy between spectra and calculations for I lies in the relative placement of the Cp levels and not the Fe–B_2H_5 level. The focus of this work lies in the nature of the interactions of B_2H_5 and C_2H_4 with Fe, and it is pleasing that here both experiment and theory provide consonant descriptions of the electronic structures in terms of IP's and MO energies.

Model Compound Comparisons. Information on the net metal–boron interaction in I may be obtained from both empirical and theoretical model compound comparisons.

I vs. B_2H_6. As indicated in Chart I, the Fp fragment in I (Figure 2) formally replaces a bridging hydrogen in B_2H_6. Thus the Fp–B interaction IP (11.4 eV) may be compared with the ionization of the MO of b_{2u} symmetry in B_2H_6 (large boron and bridging hydrogen character) at 14.7 eV.[8] The 3.3-eV decrease in IP in going from B_2H_6 to I is reasonable in terms of the much longer Fe–B distances relative to B–H (bridge) distance. The same view emerges from a comparison of calculated eigenvalues for I and B_2H_6. In Figure 7 we compare the eigenvalue spectra for I and B_2H_6 with the energy scales adjusted such that the ligand-centered orbitals have approximately the same energy. The relative destabilization (5.7 eV) of the b_{2u} MO on replacing H with Fp is evident. It is interesting to note that when I and B_2H_6 are compared in the same manner with $B_2H_5^-$ (Figure 7) the destabilization of the b_{2u} MO in going from B_2H_6 to $B_2H_5^-$ (7.3 eV) is only 1.6 eV larger than going from B_2H_6 to I; i.e., in this sense, the B_2H_5 fragment in I appears to behave like bridge-deprotonated B_2H_6 ($B_2H_5^-$).

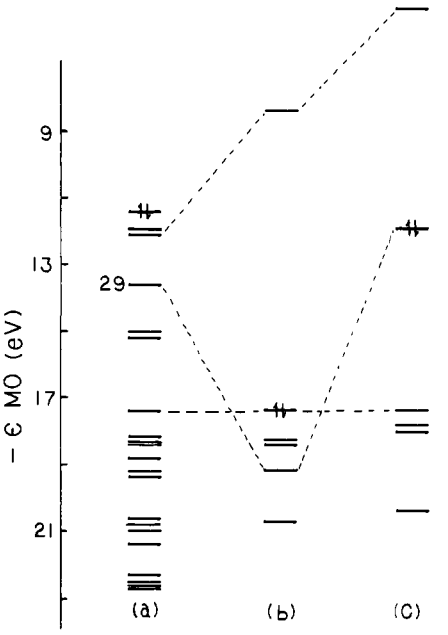

Figure 7. Comparison of the eigenvalue spectra of (a) I, (b) B_2H_6, and (c) $B_2H_5^-$. Note that the energy scales are displaced relative to each other such that the MO's with high BH terminal character have about the same energy, i.e., (b) 1.4 eV higher and (c) 7.4 eV lower in energy.

Chart I

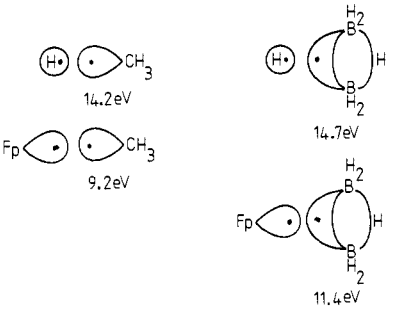

Chart II

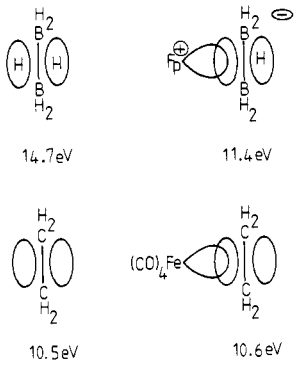

I vs. $FpCH_3$. As also indicated in Chart I, the B_2H_5 fragment in I formally replaces the CH_3 fragment in $FpCH_3$, a compound that has been the subject of several PE investigations.[14] Here the pertinent comparison is the Fe–C IP of $FpCH_3$ (9.2 eV) and the H–C IP of CH_4 (14.2 eV) relative to the analogous IP's for **I** and B_2H_6 discussed above. The significantly larger change for $FpCH_3$ vs. CH_4 (5.0 eV) relative to I vs. B_2H_6 (3.3 eV) can be rationalized in terms of a much more delocalized metal–ligand interaction in I compared to that in $FpCH_3$. That is, the Fe–B interaction in I retains significant B–H–B character such that the electron removed in this ionization feels not only the nuclear charges of Fe and the two B's but also that of the bridging H. Again, this is fully supported by the calculations. A Mulliken population analysis of the Fe–B interaction orbital (MO 29) yields 25% Fe, 49% B, and 4% H (bridge). This may be compared to the highest lying orbital of $B_2H_5^-$ (Figure 7) which contains 93% B and 5% H. The net result is a strong implication that the Fe–B interaction under discussion involves a B_2H_5 orbital that correlates with the b_{2u} MO of B_2H_6.

I vs. II. As indicated in Chart II, the iron–ligand interaction IP's of I and II can be compared by considering I as $Fp^+(B_2H_5^-)$. Consistent with the analysis above, the larger IP (11.4 eV) of I relative to that of II (10.6 eV) may be viewed as preferential stabilization of the Fe–B interaction by the bridging proton. That is, it is similar to the preferential stabilization of the b_{2u} orbital of B_2H_6 relative to the b_{2u} (π) orbital of C_2H_4 by the two bridging protons as evidenced by the IP's (14.7 and 10.5 eV).[8] This suggests that the formal comparison of I and II in Chart II in fact provides an appropriate description of the primary Fe–B bonding, i.e., a singly, bridge-protonated $B_2H_4^{2-}$ π orbital donating in a side-on fashion to the Fe atom. As this establishes empirically a relationship to the bonding of olefins to transition metals, we now proceed to a more detailed discussion of the MO properties of I and II.

Quantum Chemical Comparisons. The nature of the bonding between ethylene and a transition-metal fragment, e.g. $Fe(CO)_4$, has been well documented[11,12,17,18] and will not be repeated in detail here. However, as we wish to compare the bonding between $B_2H_5^-$ and a transition-metal fragment, e.g., Fp, with that of C_2H_4, it is first necessary to sketch the bonding in II as it appears in the Fenske–Hall approach.[19]

On being bound to a transition metal, the C_2H_4 ligand undergoes two major structural changes. First, there is an increase in the C–C bond distance, and second, the olefin substituents bend away from the metal. In the Dewar–Chatt–Duncanson bonding model,[11] both changes are associated with ligand-to-metal charge transfer from the olefin π orbital and metal-to-ligand charge transfer to the olefin π^* orbital. The bending of the substituent bonds away from the metal reflects a rehybridization at carbon

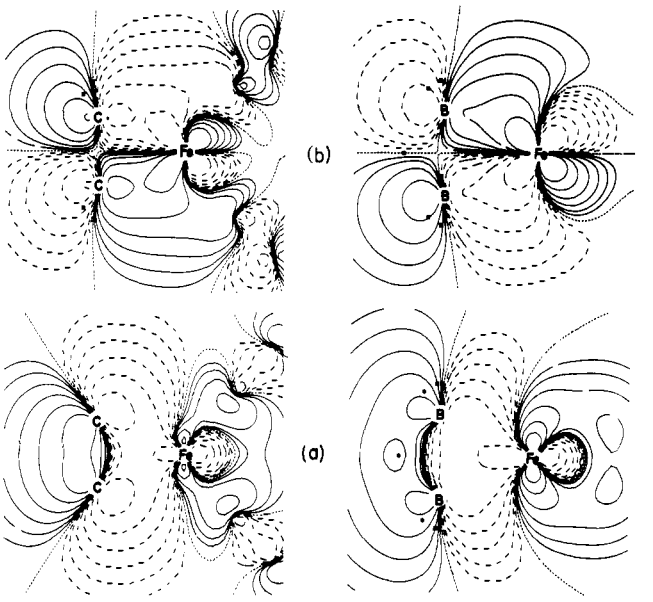

Figure 8. Amplitude contour plots in the FeX_2 plane (X = C or B) of (a) MO's 26 and 29 (see Tables I and II) for II and I, respectively, and (b) MO's 29 and 30 for II and I, respectively. In all the plots the highest contour is 0.15 electron $au^{-3/2}$, and each successive contour differs from the previous one by a factor of 2. The stars indicate H atom locations projected on the contour plane. Note that for I the dihedral angle between the FeB_2 and B_2H(bridge) planes is not 180°.

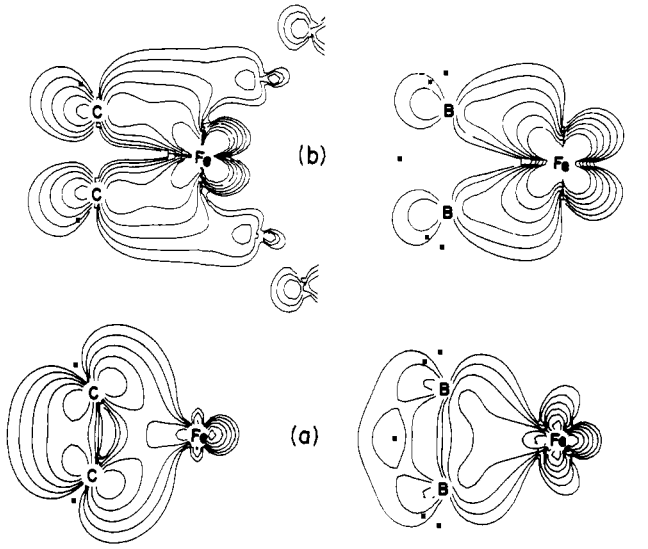

Figure 9. Density contour plots in the FeX_2 plane (X = C or B) of (a) MO's 26 and 29 (see Tables I and II) for II and I, respectively, and (b) MO's 29 and 30 for II and I, respectively. In (a) the highest contour is 0.075 electron au^{-3} while in (b) it is 0.0375 electron $au^{-3/2}$. Each successive contour differs from the previous one by a factor of 2. The stars indicate H atom locations projected on the contour plane. Note that for I the dihedral angle between the FeB_2 and B_2H(bridge) planes is not 180°.

that is thought to facilitate a stronger back-bonding interaction by increasing the overlap of the olefin π^* orbital with appropriate metal functions.[12]

The two pertinent filled MO's in the Fenske–Hall representation of the bonding in II (Table II) are MO's 26 and 29 which correlate, respectively, with the π and π^* of free C_2H_4 (Figure 6). According to a Mulliken analysis, the C_2H_4 characters in the two MO's are 81% and 34%, respectively. Amplitude and density contour diagrams of these two orbitals in the FeC_2 plane are shown on the left-hand sides of Figures 8 and 9. The family ties of MO 26 and 29 with the π and π^* of C_2H_4 are clear in the amplitude contours while the greater ligand character of MO 26 and greater

(17) Albright, T. A.; Hoffmann, R.; Thibeault, J. C.; Thorn, D. L. *J. Am. Chem. Soc.* **1979**, *101*, 3801.
(18) Calabro, D. C.; Lichtenberger, D. L. *J. Am. Chem. Soc.* **1981**, *103*, 6846.
(19) Other calculations on II have been published. Baerends, E. J.; Oudshoorn, Ch.; Oskam, A. *J. Electron Spectros. Relat. Phoneom.* **1975**, *6*, 259.

Chart III

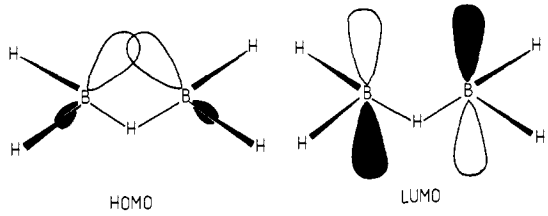

Table III. Mulliken Charges from Fenske-Hall Calculations

atom	charge	atom	charge
$(\eta\text{-}C_5H_5)(CO)_2FeB_2H_5$		$B_2H_5^-$	
B	−0.32	B	−0.45
H_t	−0.04	H_t	−0.06
H_{br}	0.16	H_{br}	0.11
Fe	0.72		
CO	0.08		
C_5H_5	−0.25		
$C_2H_4Fe(CO)_4$		C_2H_4	
C	−0.19	C	−0.05
H	0.00	H	0.03
Fe	−0.08		
CO(eq)	0.05		
CO(ax)	0.10		

metal character of MO 29 are evident in the density contours. For reference in the coming discussion, note should be taken of the distinct tilt of the carbon 2p orbitals in MO 26 *away* from the iron atom position.

In contrast to the situation with C_2H_4, the B_2H_5 fragment in I has nearly the same B–B distance as free B_2H_6, i.e., 1.80 Å, viz., 1.77 Å,[1,3] respectively. In addition there is only a small bending of the terminal hydrogens away from the metal. But like II, the Fenske–Hall results (Table I) show that there are two MO's (29 and 30) that have both boron and iron character. These orbitals correlate (Figure 6) with the HOMO and LUMO (highest occupied and lowest unoccupied MO's) of $B_2H_5^-$ which are sketched in Chart III. According to a Mulliken analysis, the B_2H_5 characters are 56% and 12%, respectively. Amplitude and density contour diagrams of these two orbitals in the FeB_2 plane are shown on the right-hand sides of Figures 8 and 9. The amplitude contours nicely display the connection of orbitals 29 and 30 with the HOMO and LUMO of $B_2H_5^-$. As the HOMO and LUMO of $B_2H_5^-$ are related to the π and π^* orbitals of C_2H_4, there is a qualitative, yet detailed analogy between the MO descriptions of the interaction of $B_2H_5^-$ and C_2H_4 with iron.

On the other hand, the interaction of $B_2H_5^-$ with iron is by no means identical with that of C_2H_4. In terms of structure, the change in the B–B distance upon complexation is small relative to the observed change for the CC distance, and the bending away of the hydrogens from the metal is much less pronounced in I than in II. This causes a large difference in the extent of orbital reorganization in going from the free to the bound ligand for $B_2H_5^-$ and C_2H_4. Whereas the orbital energies of the HOMO and LUMO of the free and bound forms of $B_2H_5^-$ are virtually the same (Figure 6), those of C_2H_4 are substantially different. Another significant structural difference is the fact that the B–B distance in II is about 0.4 Å longer than the C–C distance in I.

Perhaps the most dramatic difference lies in the charge distributions in the orbital pairs constituting the description of the metal–ligand interactions (Figure 9 and Table III). Whereas the $B_2H_5^-$(HOMO)–iron and the C_2H_4(LUMO)–iron interaction orbitals have comparable ligand and metal fragment characters, the $B_2H_5^-$(LUMO)–iron interaction orbital has mainly metal fragment character and the C_2H_4(HOMO)–iron interaction orbital has mainly ligand character. This is consistent with the higher overall energy of the donor and acceptor orbitals of $B_2H_5^-$ relative to the metal acceptor and donor orbital vs. a similar comparison for C_2H_4. Thus the relative contribution of the $B_2H_5^-$(LUMO)–iron interaction orbital to Fe–B bonding is less than

Chart IV

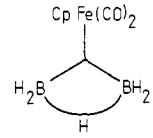

that of the C_2H_4(LUMO)–iron interaction orbital to Fe–C bonding. Second, as a consequence of the pronounced tilt of the C 2p orbitals in the C_2H_4(HOMO)–iron interaction orbital away from the iron atom, the Fe–C bonding density lies to a large extent *outside* the FeC_2 triangle. On the otherhand, it appears that the bridging hydrogen character in the $B_2H_5^-$(HOMO)–iron interaction orbital causes a tilt of the B 2p orbitals toward the iron atom such that the Fe–B bonding density lies mostly *inside* the FeB_2 triangle. In fact the density contours seem to define, in the terminology of Lipscomb, a closed three-bond.[20] Hence, a very reasonable but simple representation of the Fe–B bonding in I is given by Chart IV.

It is important to note that although there is no tilting of the C 2p π components of either HOMO or LUMO in free C_2H_4, the presence of the bridging hydrogen in $B_2H_5^-$ causes a rehybridization at boron such that, even when the terminal hydrogens and borons are coplanar as in the free ligand, the B sp^x hybrids of the HOMO point almost directly at the potential metal position. There is no similar tilting of the LUMO as the bridging hydrogen lies on a nodal plane. This orienting effect of the bridging hydrogen on the HOMO of $B_2H_5^-$ appears to neatly compensate for the longer B–B distance relative to that of C–C in C_2H_4.

A final comparison of I and II appears in Table III, where the results of a Mulliken charge analysis are presented for the complexes as well as the free ligands. The C_2H_4 picks up a small amount of electronic charge on being bound to $Fe(CO)_4$ presumably reflecting the importance of M → L back-bonding. On the other hand, $B_2H_5^-$ loses a small amount of charge which, assuming $B_2H_5^-$ is the free ligand, is consistent with a less important role for a back-bonding interaction. For I the metal atom is more positively charged than for II; however, as the metal fragments are different no great significance can be placed on these charges.

Other Borane Analogues of π Hydrocarbon Ligands. One of the striking features of the comparison of C_2H_4 as a π ligand with $B_2H_5^-$ as an analogous ligand is the directionality induced in the HOMO of the latter by the presence of the bridging hydrogen. This directionality, which is present even in the undistorted free ligand, appears to facilitate the formation of a closed, three-center bond with the transition metal through which the major metal–boron interaction takes place. The question now arises as to whether this is a general phenomenon. In fact, we have already pointed out that in a qualitative MO study of the ligand properties of triboranes, the "borallyl" ligand (B_3H_7 in a configuration analogous to a π allyl ligand Figure 1) exhibits significant tilting of the in-phase "π" orbital toward the potential metal site on the side of the borane fragment opposite to the bridging hydrogens.[22] To probe the generality of this role of the bridging hydrogens in other borane metal complexes, we have applied the extended Hückel technique to all the borane ligands shown in Figure 1.

The borane ligands are given idealized structures with the borons and terminal hydrogens coplanar and the bridging hydrogens all on one side of the boron plane (Figure 1). In this form, the boranes closely approximate the known or proposed structures of these fragments in characterized complexes. The results from the extended Hückel calculations are summarized in Figure 10 and Table IV. In all cases the frontier orbitals of the borane ligands are similar to those of the analogous hydrocarbons. That is to say they are basically constructed of out-of-plane B 2*p* functions having the same nodal patterns as the hydrocarbon π systems. However, in each case, the presence of bridging hy-

(20) Lipscomb, W. N. "Boron Hydrides"; Benjamin: New York, 1963.
(21) DeKock, R. L.; Fehlner, T. P. *Polyhedron*, in press.
(22) Housecroft, C. E.; Fehlner, T. P. *Inorg. Chem.* **1982**, *21*, 1739.

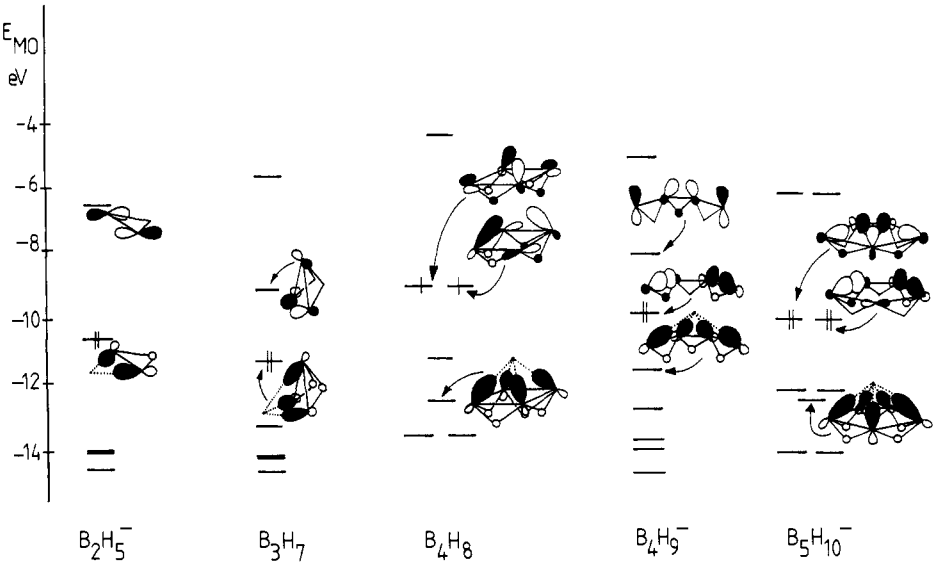

Figure 10. Frontier orbitals for borane "π" ligands according to the extended Hückel method. The HOMO is indicated by the vertical lines representing the electron population.

Table IV. Out-of-Plane Tilt Angles (deg) for Frontier Orbitals[a]

	LUMO	HOMO	symmetric MO[b]
$B_2H_5^-$	90	52	
B_3H_7	68	50	
B_4H_8	90	71	49
$B_4H_9^-$	68	52	49
$B_5H_{10}^{-}$ [c]		52	50

[a] Orbitals are depicted in Figure 10. Where orbitals for individual atoms vary in their degrees of tilt within one MO, an average value of tilt angle is given. Angle is defined in Chart V. [b] The symmetric MO pointing to a potential metal fragment where not coincident with HOMO. See Figure 10. [c] LUMO is not included.

Chart V

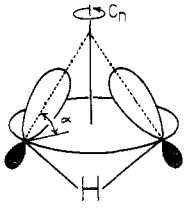

drogens causes the frontier orbitals to possess significant in-plane character. This shows up as significant inward tilting of these orbitals toward a point near the major out-of-plane symmetry axis on the side of the ligand plane opposite the bridging hydrogens Chart V. As indicated in Table III, the extent of this tilting decreases as the number of nodes in the orbital increases, thereby matching the requirements of a metal fragment orbitals. That is, the metal d_{z^2} lying on the symmetry axis interacts with the symmetric, most tilted borane orbital whereas the metal d_{xz} and d_{yz} interact with the higher, less tilted borane orbitals. This is illustrated for the two major types of Fe–B interaction orbitals in $(CO)_3FeB_4H_8$ in Figure 11. In a real sense the tilting compensates for the fact that the borane fragments are all significantly larger than their hydrocarbon counterparts, i.e., the B–B distances are about 0.4 Å larger than the analogous C–C bonded distances. It is amusing to note that for $B_4H_9^-$ the tilting of the frontier orbitals changes with BBB angle such that the sp^x hybrids on the terminal borons track the point corresponding to the potential metal position.

The similarity in bonding found for $B_2H_5^-$ and C_2H_4 in I and II appears to carry through to the higher homologues. Likewise, the role of the bridging hydrogen in $B_2H_5^-$ in modifying the spatial orientation of the donor orbital to enhance the metal–boron in-

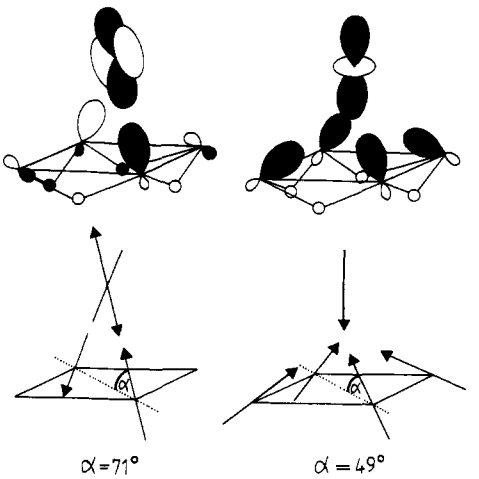

Figure 11. Schematic representation of the principal Fe–B interaction orbitals for $(CO)_3FeB_4H_8$ showing the tilt of the borane ligand orbitals with respect to the ligand plane.

teraction, also carries over to the higher homologues. It is worthwhile to note that the effect of out-of-plane bridging hydrogens does not appear to be restricted to boranes. We have pointed out in other work that a major effect of out-of-plane bridging hydrogens on a triangular iron ring composed of $Fe(CO)_3$ fragments relative to an isoelectronic cobalt ring is to cause an increased tilting of the octahedral bond vector toward a point on the side of the metal plane opposite the bridging hydrogens.[9] Thus, in all these systems the bridging hydrogen is present as much more than an innocent spectator.

Experimental Section

The sample of I was prepared as described elsewhere.[3] Photoelectron spectra were recorded at room temperature with both He I (21.2 eV) and Ne I (16.8 eV) radiation. The spectrometer has been described earlier[23] and was operated in the energy analyzer scan mode with an effective resolution of 0.030 V at a 5-eV pass energy. A mixture of xenon and argon was used to calibrate the energy scale.

For the calculations, the geometries of I and II were taken from known X-ray structural data but idealized to C_{2v} symmetry.[3,24] All C–O bond lengths were set at 1.13 Å and Fe–CO bond lengths at 1.80 Å. The known geometries of C_2H_4 and B_2H_6[20] were used and the geometry of $B_2H_5^-$ was assumed to be that of B_2H_6 less a bridging proton. The geometries of the larger borane ligands were all idealized with B–H

(23) Fehlner, T. P. *Inorg. Chem.* **1975**, *14*, 934.
(24) Ittel, S. D.; Ibers, J. A. *Adv. Organomet. Chem.* **1976**, *14*, 33.

(terminal) = 1.19 Å, B-B = 1.80 Å, B-H(bridge) = 1.32 Å with all borons and terminal hydrogens lying in a plane and the dihedral angle of the boron plane with the B-H-B plane being 90°. For $B_4H_9^-$, the B-B-B angle was chosen to be 120°.

The Fenske-Hall calculations[15] employed single-ζ Slater basis functions for the 1s and 2s function of B, C, and O. The exponents were obtained by curve fitting the double-ζ functions of Clementi[25] while maintaining orthogonal functions; the double-ζ functions were used directly for the 2p orbitals. For hydrogen, an exponent of 1.16 was used which corresponds to the minimum energy exponent for methane.[26] The iron 1s-3d functions were taken from the results of Richardson et al.[27] and were all single-ζ except the 3*d* function which is double-ζ and was chosen for the 1+ oxidation state. Both the 4s and 4p exponents were chosen to be 2.0. For all the atoms used here, these are the basic functions typically employed by Fenske and Hall in their studies using this quantum chemical approach.

The extended Hückel calculations[28] employed Slater functions, and the orbital exponents and diagonal matrix elements used are the same as those used previously.[29] The arithmetic mean Wolfsberg-Hemholz approximation with $K = 1.75$ was used.

Acknowledgment. The support of the National Science Foundation is gratefully acknowledged as is the computing time provided by the Notre Dame Computing Center.

Registry No. I, 72576-54-6; II, 32799-25-0.

(25) Clementi, E. *J. Chem. Phys.* **1964**, *40*, 1944.
(26) Hehre, W. J.; Stewart, R. F.; Pople, J. A. *J. Chem. Phys.* **1969**, *51*, 2657.
(27) Richardson, J. W.; Nieupoort, W. C.; Powell, R. R.; Edgell, W. F. *J. Chem. Phys.* **1962**, *36*, 1057.
(28) Hoffmann, R. *J. Chem. Phys.* **1963**, *39*, 1397. Hoffmann, R.; Lipscomb, W. N. *Ibid.* **1962**, *36*, 3489. Hoffmann, R.; Lipscomb, W. N. *Ibid.* **1962**, *37*, 2872.
(29) Andersen, E. L.; DeKock, R. L.; Fehlner, T. P. *Inorg. Chem.* **1981**, *20*, 3291.

Mechanisms of $Re_2(CO)_{10}$ Substitution Reactions: Crossover Experiments with $^{185}Re_2(CO)_{10}$ and $^{187}Re_2(CO)_{10}$

A. M. Stolzenberg and E. L. Muetterties*

Contribution from the Department of Chemistry, University of California, and the Materials and Molecular Research Laboratory, Lawrence Berkeley Laboratory, Berkeley, California 94720.
Received August 9, 1982

Abstract: $^{185}Re_2(CO)_{10}$ and $^{187}Re_2(CO)_{10}$ were prepared separately and then utilized in combination in crossover experiments to probe for fragmentation to mononuclear rhenium species in thermal and photochemically initiated substitution reactions. For the CO-$Re_2(CO)_{10}$ exchange reaction, a reaction separately analyzed for ^{13}CO-^{12}CO interchange, no crossover was observed at 150 °C after 14 half-lives of reaction (14 h). Similarly, the thermal reaction sequences of $Re_2(CO)_{10} + P(C_6H_5)_3 \rightleftharpoons Re_2(CO)_9P(C_6H_5)_3 + CO$ and $Re_2(CO)_9P(C_6H_5)_3 + P(C_6H_5)_3 \rightleftharpoons Re_2(CO)_8[P(C_6H_5)_3]_2 + CO$ were examined at 150 °C (maintaining a CO pressure of ~560-640 mm). No crossover was detectable in either $Re_2(CO)_{10}$ or $Re_2(CO)_9P(C_6H_5)_3$ (relative to blank experiments). Hence, phosphine substitution reactions proceed without a detectable formation of mononuclear rhenium species. These observations support a CO dissociative mechanism. A model based upon this mechanism can accurately reproduce the mass spectra observed during ^{13}CO-^{12}CO interchange. In the absence of a CO atmosphere, $^{185}Re_2(CO)_{10}$ and $^{187}Re_2(CO)_{10}$ formed $^{185}Re^{187}Re(CO)_{10}$, and this interchange was nearly complete at 150 °C within 14-16 half-lives. All photochemically initiated reactions with the two labeled decacarbonyls led to complete crossover within short reaction times. It appears then that the primary mode of reaction for $Re_2(CO)_{10}$ under photolysis conditions involves Re-Re bond scission as an early elementary step. Also, the reversible steps leading to the precursor(s) to $Re_2(CO)_{10}$ decomposition include scission of the rhenium-rhenium bond.

Important to a full development of metal cluster chemistry is a basic understanding of reaction mechanism. Because of the very complexity of these polynuclear species, the number of chemically plausible reaction pathways for a given system can be relatively large.[1] In metal carbonyl clusters, the average metal-metal and metal-carbonyl bond energies appear comparable. Hence, scission of *either* type of bond can be an elementary step in even simple reactions like ligand replacement. We address here the mechanism of $M_2(CO)_{10}$ reactions.

Despite substantial efforts, the mechanism of substitution reactions of group 7 metal carbonyl dimers remains an unresolved question.[1a] Two different mechanisms have been advanced. One involves reversible CO dissociation, Scheme I; the other reversible metal-metal bond homolysis, Scheme II. Both mechanisms predict rate expressions that are first order in metal-carbonyl dimer concentration and independent of entering ligand concentration (when the concentration of the entering ligand is sufficiently large that the reverse of the activation step is negligible). In contradistinction to the CO dissociative mechanism, the radical mechanism requires the dependence on metal-carbonyl dimer concentration to decrease from first to half-order for less than limiting rates. Less than first-order kinetic behavior has not yet been observed for any ligand substitution reaction. However, Poë and co-workers have reported such behavior for the presumedly related decomposition reactions of $M_2(CO)_{10}$ that occur at the same rates as ligand substitution and therefore favor a radical mechanism.[2-11] Sonnenberger and Atwood favor a CO disso-

(1) (a) For a recent review of cluster reaction mechanism, see: Muetterties, E. L.; Burch, R. R.; Stolzenberg, A. M. *Annu. Rev. Phys. Chem.* **1982**, *33*, 89. (b) For a recent study of contributing electronic and steric factors in such substitution reactions, see: Darensbourg, D. J.; Baldwin-Zuschke, B. J. *J. Am. Chem. Soc.* **1982**, *104*, 3906. (c) For a seminal study supporting CO dissociation, see: Wawarsik, H.; Basolo, F. *Inorg. Chim. Acta* **1968**, *3*, 113.
(2) Haines, L. I. B.; Hopgood, P.; Poë, A. J. *J. Chem. Soc. A* **1968**, 421.
(3) Haines, L. I. B.; Poë, A. J. *J. Chem. Soc. A* **1969**, 2826.
(4) Fawcett, J. P.; Poë, A. J.; Sharma, K. R. *J. Am. Chem. Soc.* **1976**, *98*, 1401.
(5) Fawcett, J. P.; Poë, A. J. *J. Chem. Soc., Dalton Trans.* **1976**, 2039.
(6) DeWit, D. G.; Fawcett, J. P.; Poë, A. J. *J. Chem. Soc., Dalton Trans.* **1976**, 528.
(7) Fawcett, J. P.; Poë, A. J. *J. Chem. Soc., Dalton Trans.* **1977**, 1302.
(8) Cowdhury, D. M.; Poë, A. J.; Sharma, K. R. *J. Chem. Soc., Dalton Trans.* **1977**, 2352.

0002-7863/83/1505-0822$01.50/0